MINISTRY OF EDUCATION AND TRAINING
HCMC UNIVERSITY OF TECHNOLOGY AND EDUCATION

DEVELOPMENT OF A BREAST CANCER DIAGNOSTIC SUPPORT SYSTEM USING ARTIFICIAL INTELLIGENCE

Major: Electronic Engineering
Major Code: 9520203

SUMMARY OF DOCTORAL THESIS

HO CHI MINH CITY – 2025

The study was completed at Ho Chi Minh City University of Technology and Education

Scientific supervisor 1: Associate Professor, Dr. ----------

Reviewer 1:
Reviewer 2:
Reviewer 3:

The thesis has been defended before the Thesis Evaluation Council at the Grassroots Level meeting at Ho Chi Minh City University of Technical Education on 01 Nov 2025

LIST OF PUBLISHED PAPERS

1. T.-T. Nguyen, T.-H. Nguyen, B.-V. Ngo, and T.-N. Nguyen, "Largest roi segmentation for breast cancer classification using a VGG16 deep learning network," Advances in Electrical and Electronic Engineering, 2024, DOI: 10.15598/aeee.v22i4.240303.

2. Thanh-Tam Nguyen, Thanh-Hai Nguyen, "Segmentation and Color ROI Extraction from Breast Imaging Datasets for Cancer Classification", Engineering, Technology and Applied Science Research, 2025, DOI: 10.48084/etasr.12067.

3. Thanh-Nghia Nguyen, Thanh-Tam Nguyen, Thanh-Hai Nguyen, .V. Ngo, "A Robust Approach for Breast Cancer Classification from DICOM Images", Engineering, Technology and Applied Science Research, 04 Jun 2025, Vol. 15, Issue 3, pages 23499 – 23505, doi:10.48084/etasr.10931.

4. Thanh-Tam Nguyen, Nguyen Thanh Hai, Tin-Trung Nguyen, "Design of A Telemedicine System for Classification of Breast Cancer Images", Journal of Technical Education Science, 2025, DOI: 10.54644/jte.2025.1969.

5. T.-T. Nguyen, T.-H. Nguyen, B.-V. Ngo, and D.-D. Vo, "Breast Image Segmentation for evaluation of Cancer Disease," in 2020 5th International Conference on Green Technology and Sustainable Development (GTSD), 2020, pp. 344–348, doi: 10.1109/GTSD50082.2020.9303133.

6. T.-T. Nguyen, T.-H. Nguyen, and B.-V. Ngo, "A GLCM Algorithm for Optimal Features of Mammographic Images for Detection of Breast Cancer," in 2021 International Conference on System Science and Engineering (ICSSE), 2021, pp. 295–299, doi: 10.1109/ICSSE52999.2021.9538426.

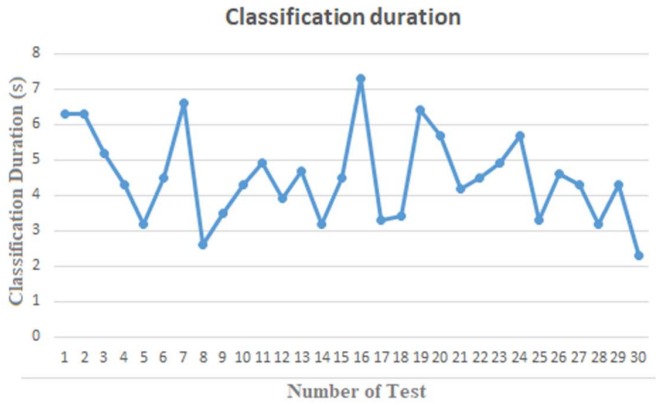

Figure 8. Classification time measurement results.

Figure 8 shows that the average classification time of the system is 4.5 seconds (fastest 2.3 seconds, slowest 7.3 seconds) after 30 trials. The EfficientNet-B7 system trained on DICOM data from Ho Chi Minh City Oncology Hospital achieved 97% accuracy on the training set and 89.58% on the testing set, meeting the requirements for practical deployment with a transmission speed of 284 Mbps.

CHAPTER 6 CONCLUSION AND DEVELOPMENT DIRECTIONS

The thesis focuses on enhancement algorithms and pre-processing of mammograms to improve image quality, thereby improving the accuracy of classification between lesions and non-lesions. The research data includes more than 4,000 images from Ho Chi Minh City Oncology Hospital, which have been processed and labeled according to standards. The methods of feature extraction, ROI segmentation and image coloring (CROI) help improve 6-8% accuracy, reaching nearly 95% in lesion classification and 92.6% in cancer risk classification according to BIRADS. The thesis also builds deep learning models combined with advanced CNNs, and develops a remote diagnosis support system for doctors. Experimental results on many data sets show clear effectiveness, published in scientific journals (Q2, Q3), contributing to early detection and support for breast cancer diagnosis in telemedicine.

CHAPTER 1 OVERVIEW

1.1 OVERVIEW

Breast cancer is the leading cause of death in women, with the number of cases increasing, even in young people in Vietnam. Each year there are about 22,000 new cases and more than 9,000 deaths, of which nearly 70% are detected at a late stage, mainly due to the lack of screening systems and limited medical resources. Bach Mai Hospital receives more than 5,000 patients/day, creating great pressure on doctors, easily leading to misdiagnosis.

The solution is to integrate AI into the remote diagnosis system, which helps increase accuracy up to 94.5% (compared to the traditional 88%) and reduce the number of direct examinations by about 40%. In Vietnam, where the rate of late detection is still very high, this technology promises to improve access and quality of health care.

1.2 RESEARCH OBJECTIVES

1.2.1 Research objectives

Development of an artificial intelligence-based UTV disease diagnosis system trained through various large sets of processed X-ray images to standardize to assist physicians in diagnosing UTV disease.

1.2.2 Specific objectives

Based on the research objectives, the topic will be divided into 3 specific objectives to achieve the set goals:

Objective 1: Collect large datasets of various mammograms (ranging from about five thousand to nearly ten thousand images) that have been labeled. On those image sets, develop image processing algorithms before extracting image features for abnormality detection of mammograms.

Objective 2: Build an algorithm using artificial intelligence to predict the patient's UTV disease status (with or without disease) based on the input image datasets obtained.

Objective 3: Deploy a remote diagnosis system model using AI that allows doctors to upload mammograms for remote prediction of breast cancer status via phone or PC, thereby supporting doctors in making diagnosis results. Through this system, we can collect data and results on breast cancer of patients in Vietnam.

CHAPTER 2 LITERATURE REVIEW

2.1 BREAST CANCER IMAGING DATASETS

MIAS [63]: More than 300 mammograms annotated with background tissue type, abnormality and severity, along with X, Y coordinates of the lesion [64].

DDSM [65]: Includes more than 2,600 mammography studies from film scans. The CBIS-DDSM [66] subset is annotated in detail for tumor type, grade, and stage.

INBreast [67]: Provides more than 410 high-quality digital mammograms to support breast cancer research.

BCDR [68]: Focus on full-field digital mammography (FFDM), encouraging contributions from the research community [69].

BancoWeb LAPIMO [70]: Includes more than 1,400 TIFF images from 320 patients, part of the BancoWeb LAPIMO project.

VICTRE [71]: A simulated dataset with 2,986 subjects representing a wide range of breast sizes and densities.

OPTIMAM (OMI-DB) [71]: A fully annotated mammography database focused on research purposes.

2.2 IMAGE SEGMENTATION AND IMAGE PROCESSING IN UTV IMAGES

Image segmentation

Mammograms are often uneven and contain a lot of noise, so studies often apply preprocessing algorithms to improve quality and increase classification efficiency with deep learning networks such as VGG16, EfficientNet. At this stage, common steps include noise filtering, removing unimportant components (pectoral muscles, labels, etc.) and background extraction using methods such as Otsu thresholding. After preprocessing, the image is segmented to determine suspicious regions (ROIs) using many techniques: based on thresholding, regions, features, edges, or deep learning. These methods help remove background, retain tumors and improve detection sensitivity. In particular, Otsu thresholding is a popular technique in medical images, giving segmentation results up to 77.43%, and is applied in this study to extract ROIs from mammograms with four types of lesions.

Improving image quality in UTV diagnosis

Table 4. Representation of classification results using confusion matrix.

Categories	Number of Images	True Positive	False Positive	
Normal	160	144	7 to Benign	9 to Malignant
Benign	160	141	8 to Normal	11 to Malignant
Malignant	160	145	9 to Normal	6 to Benign

The analysis of the training results shows that the AI model with EfficientNet-B7 achieves high training accuracy, especially converging at around 97%, showing good learning ability on the training data. However, the accuracy on the test set is only around 89.58%, which may be a minor issue related to the construction of new data. The difference between the training and test accuracy may be due to the fact that the data sets used are real data, which have large differences in quality and are collected from different devices. The accuracy and F1 score are shown in Table 5.

Table 5. *Representation of the precision and F1-score.*

Categories	Precision	recall	f1-score
Normal	0.8944	0.9000	0.8972
Benign	0.9156	0.8812	0.8981
Malignant	0.8788	0.9062	0.8923

Results of the Telemedicine Model

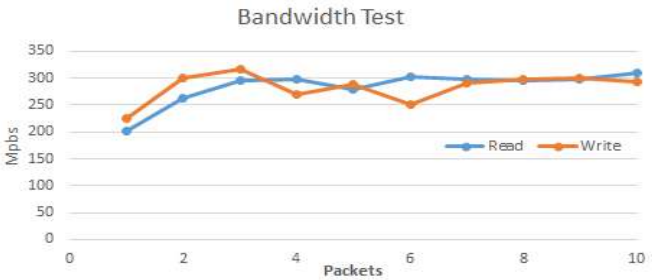

Figure 7. System bandwidth measurement results.

Figure 7 shows the test results of the telemedicine system. Specifically, the chart shows that the system's read/write speed always exceeds the allowable threshold of 200Mbps and the average speed is 284Mbps.

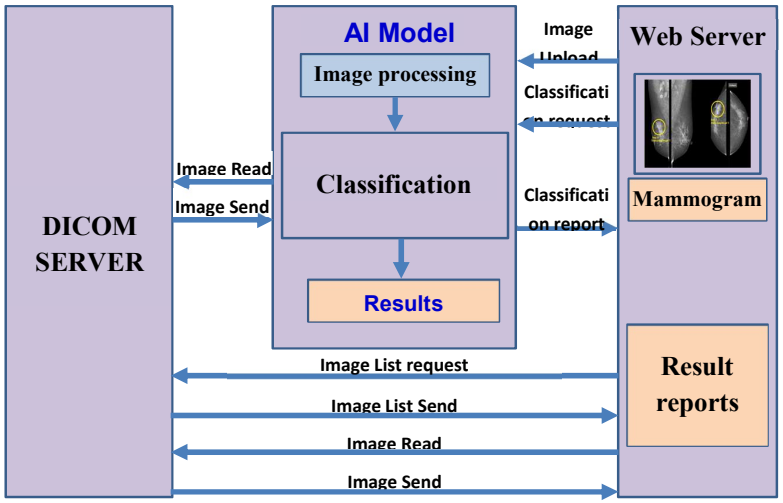

Figure 3. Depicts the internal protocols for information exchange between the three main components in the system core.

Result

Breast cancer classification results

The classification accuracy is evaluated through the confusion matrix, in which the image sets collected from Ho Chi Minh City Oncology Hospital and the test dataset are completely independent of the training dataset, with a ratio of 8:2. Basically, there are 3 types of image sets: Benign, Malignant and Normal. Therefore, the training results of the EfficientNet-B7 model are evaluated by the Loss and Accuracy functions.

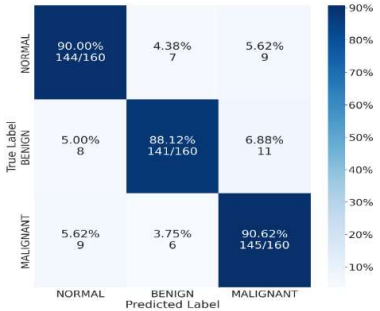

Figure 6. Confusion matrix representation for three lesion types such as benign, malignant and normal.

Diagnostic accuracy depends largely on the quality of mammograms. Clear images help AI detect microscopic lesions more effectively. To improve image quality and contrast, many image enhancement techniques have been studied, including: traditional methods, region-based enhancement, feature-based enhancement (such as wavelet transform), and fuzzy entropy enhancement. These techniques help clarify microcalcifications, tumors, contours, and image details, but can increase noise.

Recent studies have demonstrated its effectiveness: Shenbagavalli achieved 93.45% accuracy with shearlet transform; Teare used CLAHE combining CNN and random forest, achieving sensitivity of 0.91 and specificity of 0.80. In addition, FADHECAL technique reduces noise while preserving image details better than other methods. Recently, advanced fuzzy set-based enhancement methods and optimization algorithms have also shown promising results. Overall, improving image quality is an important step to help AI systems and radiologists make more accurate diagnoses.

2.3 UTV IMAGE CLASSIFICATION USING MACHINE LEARNING

Detection and classification of breast tumors

Tumors are the most common symptom of breast cancer, but detection on mammograms, especially in dense breast tissue, is quite difficult. Many studies have applied AI to improve accuracy. Typical methods include: visual fuzzy clustering (CrSA-IFCM-NA), multi-layer CNN, YOLO, Fast-RCNN, U-Net, Mask-RCNN, and hybrid models combining deep learning with ML.

The reported results are very promising: the detection accuracy can reach 98.96% with YOLO and FrCN on INBreast, 100% sensitivity and 94% specificity with YOLO, or AUC 0.95 with Fast-RCNN. In addition, many studies have also focused on benign/malignant classification using CNN, hybrid deep learning, and deep fusion learning, with accuracy ranging from 89% to over 99%. New methods also focus on the interpretability of the results, such as the combination of U-Net and Case-Based Reasoning.

UTV Risk Assessment

Some studies have focused on classifying breast density (according to BIRADS) using CNN, residual CNN or unsupervised learning with autoencoder. In addition, deep learning models are also used to classify benign/malignant tumors, with strategies such as transfer learning, data augmentation, or hybrid models combining DL and ML, giving high accuracy. The problem of limited and imbalanced data is overcome by generating synthetic data (cGAN) or multi-task learning. Google's research (2020, Nature) shows that AI can diagnose breast

cancer from mammograms with the same or better accuracy than experts, while reducing false positives and negatives.

In addition to imaging, many ML models (SVM, ANN, CBR…) have also been applied to predict risk based on clinical and epidemiological factors. In particular, studies using routine mammography to estimate risk in community screening groups showed that FFDM-based AI predicted breast density better than BIRADS and traditional epidemiological models (AUC 0.60–0.84).

CHAPTER 3 Mammagram Image Acquisition and Preprocessing

3.1 VINDR-MAMMO DATASET

VinDr-Mammo dataset [135]: in which mammograms were collected from 2018 to 2020. In particular, these image sets are stored at the PACS System of Hanoi Medical University Hospital (HMU) and Hospital 108 (H108). All 20,000 mammograms in the VinDr-Mammo dataset are classified into five mammogram groups and 11 breast disturbances (tumor; suspicious calcification; asymmetry; localized asymmetry; global asymmetry; structural distortion; skin thickening; skin retraction; nipple retraction; and suspicious lymph nodes), in which patients are aged from 20 to 86 and are most concentrated in the 40-45 age group.

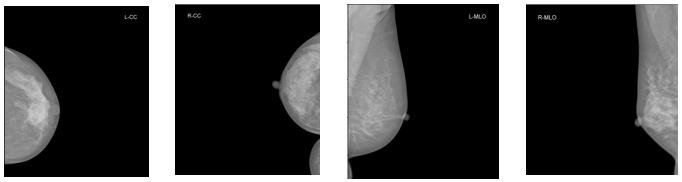

(a) (b) (c) (d)

Figure 3. 1. A sample image set of VinDr-Mammo dataset : (a) Left CC; (b) Right CC; (c) Left MLO; (d) Right MLO

Table 3. 1Vindr-Mammo Dataset Information

Type of injury	Number of photos
Tumor	1,226
Calcification	543
Focal asymmetry	269
Structural deformation	119
Normal	2,551

5.3 REMOTE DIAGNOSTIC SUPPORT SYSTEM USING DEEP LEARNING NETWORK

The system operates on a web platform, allowing doctors to easily access it via multiple devices, while ensuring security and compatibility. The main requirements include: (1) anytime, anywhere access via the internet; (2) DICOM and JPEG support; (3) communication via a web interface; (4) providing results of lesion classification and risk level.

2.1. Hardware architecture of the telemedicine system

The figure below illustrates a proposed system for remote breast cancer image classification. The system consists of core components, interacting peripherals, and connections between them. Specifically, the system consists of three main components: 1. Picture Archiving and Communication System (PACS) server for images; 2. Web server for data connection with AI model and PACS; 3. AI model for image classification.

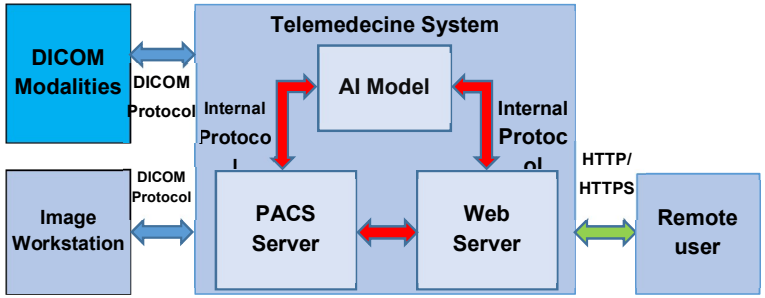

Figure 1. Illustration of the telemedicine system used to classify breast cancer images using an AI model.

Describes the internal protocols of the system core

The AI model uses internal protocols to exchange information between components and communicate with peripheral devices via popular standards such as DICOM (X-ray machines, display devices) and HTTP/HTTPS (terminals). The system connects to PACS to retrieve and process images before classification, while the web server manages data, displays and sends diagnostic requests to the AI model to return results to the user. System parameters (image size, storage capacity...) are optimized based on data and deployment requirements to ensure high performance.

collection

Table 5. 1. Number of images after enhancement of the image set

Category	Original	Augmentation/Choice	Division of image sets	
			Train	Test
BIRADS-1	13406	3000	2400	600
BIRADS-2	4676	3000	2400	600
BIRADS-3	930	3000	2400	600
BIRADS-4	762	3000	2400	600
BIRADS-5	226	3000	2400	600
Total	***20000***	***15000***	***12000***	***3000***

b) Results of breast lesion image classification according to BIRADS

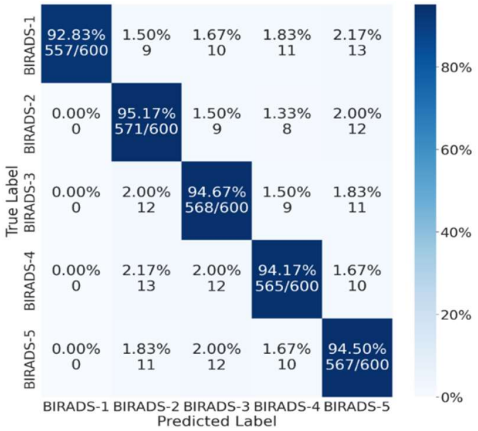

Figure 5. 5

The results show that image preprocessing (XLA) significantly improves the accuracy of UTV image classification according to BIRADS scale. In particular, image segmentation and Colormap application increase the accuracy by about 8%, while Gamma correction only improves by ~1% and Histogram equalization is almost negligible. The EfficientNet model is more suitable for color images. In the study, the system achieved an average accuracy of 92.6% and F1-score of 92.33% on VinDr-Mammo set, outperforming the previous LightGBM which only achieved 67%.

The number of images in the VinDr-Mammo dataset with different lesion types is unbalanced.

3.2 COLLECTING BREAST X-RAYS AT THE CANCER HOSPITAL

In this study, DICOM mammography images collected from the Vietnam Oncology Hospital were used. The image collection process was carried out according to a strictly designed procedure to ensure the validity of the dataset as shown in Figure 3.5. First, DICOM mammography images were collected from the hospital's PACS image storage device and anonymized to protect patient privacy. Next, the dataset was annotated by several radiologists using the hospital's computerized labeling tool. Finally, the annotated images were stored as a dataset.

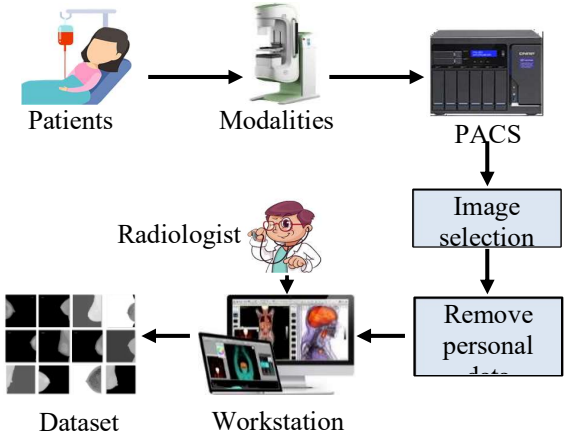

Figure 3.5 Data collection diagram at Ho Chi Minh City Oncology Hospital

In this step, more than 4000 DICOM format mammograms from the DICOM system of Ho Chi Minh City Oncology Hospital PACS, with scans between 2018 and 2023, were collected.

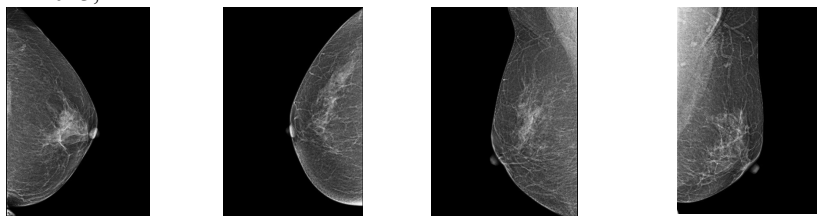

Figure 3.6 Some images from the dataset collected at Ho Chi Minh City Oncology Hospital

To ensure patient privacy is protected, patient identifiable information in the DICOM tags will be completely erased. Only necessary information used for DICOM image processing and patient age information will be retained. The parameters of the images collected at the Cancer Hospital are described in the table below.

Table 3.4 Shows detailed information of the image after collection

STT	Parameter	Value
1	Number of photos	4034
2	Image size	1024 ×1024
3	Format	DICOM
4	File size	8.8MB

For the oncology hospital dataset, labeling is done by the radiologists of the oncology hospital. After the image is taken by the technician, the radiologist will systematically analyze the X-ray image, usually in a certain order so as not to miss any details.

3.3 IMAGE ENHANCEMENT

Adjust UTV image brightness and contrast

After collecting the dataset from MIAS, the input images are enhanced using fuzzy logic and likelihood distribution algorithm.

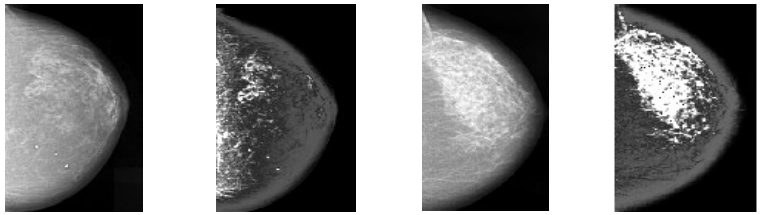

(a) (b) (c) (d)

(a) original image of normal case; (b) enhanced image of normal case; (c) original image of cancer case; (d) enhanced image of cancer case.

Figure 3.9 Representation of original and enhanced images

hospitals in Vietnam.

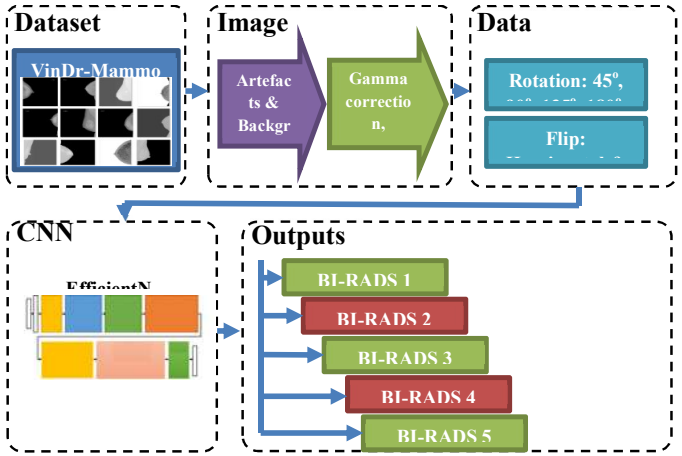

Figure 5. Block diagram of the processing of the system for classifying breast X-ray images according to the level of damage according to the BIRADS 3

Before being fed into the CNN, the images in the DL set are preprocessed by removing unnecessary information and enhancing their quality. The dataset is then expanded by rotation, flipping, and changing the brightness to balance the number of images between the lesion levels. The images are trained on EfficientNet (initialized from ImageNet), the final layers are fine-tuned, and the appropriate output layer is added. The classification results are compared to select the best performing model for classifying mammograms according to the BIRADS scale [171].

a) DL set

(a) Right CC (a) Left CC (a) Right MLO (a) Left MLO

Figure 5Set 44 images in a mammogram result of VinDr-Mammo image

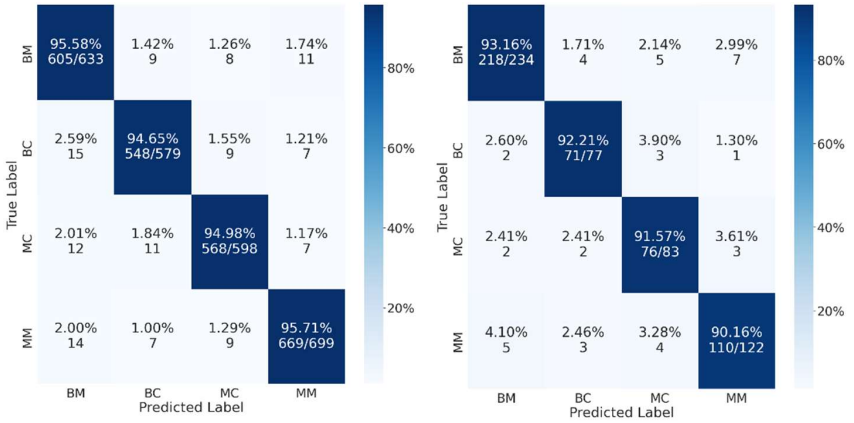

(a) (b)

Figure 5. 2. Depiction of the classification performance of two types of DL sets with Benign Calcification (BC), Benign Mass (BM), Malignant Calcification (MC), Malignant Mass (MM). (a) CBIS-DDSM DL set; (b) MIAS DL set.

The extraction of large ROIs and image enhancement have improved the classification performance of the proposed model, in particular, the model proposed in this paper achieves 95% accuracy. For high performance, image sets are extracted with large ROIs to capture many features of breast lesions, then normalized and enhanced. To evaluate the effectiveness of the proposed model, the paper presents three DL set cases as shown in Table 5.8. Among them, the image set processed according to the proposal with the largest ROI gives the highest performance of 95%, while the image set processed according to the proposed model without processing has an accuracy of 82.1% lower than that of Otsu segmentation alone. This result demonstrates that the proposed model can classify 4 types of breast lesions, making it easier to identify breast cancer through mammography with the highest accuracy.

5.2 RESULTS OF CLASSIFICATION OF BREAST CANCER ACCORDING TO BIRADS

This study aims to classify mammograms according to the BIRADS scale using the EfficientNet model combined with XLA methods, with the goal of finding the optimal processing model to support early diagnosis of breast cancer. The experiment was conducted on the VinDr-Mammo dataset [24] collected from

Gamma correction:

Gamma correction, which adjusts the brightness of an image to accentuate the transition from dark to light and vice versa using nonlinear transformations. The gamma correction algorithm is performed as follows.

Algorithm 2. Adaptive Gamma Correction

```
START
      READ original image I IN (x,y) where x and y denotes coordinates of the pixel
      Select Gamma initial value γ0
      WHILE NOT CorrectGamma(I OUT (x,y))
            Apply Gamma correction I OUT (x,y) = I IN (x,y)^γ
      END WHILE
      OUTPUT I OUT (x,y)
END
```

Figure 3.10 below shows the result of performing gamma correction on an image with the background and unwanted artifacts removed. The Adaptive Gamma correction algorithm helps to unify the image quality and eliminate differences caused by the acquisition device on the mammograms.

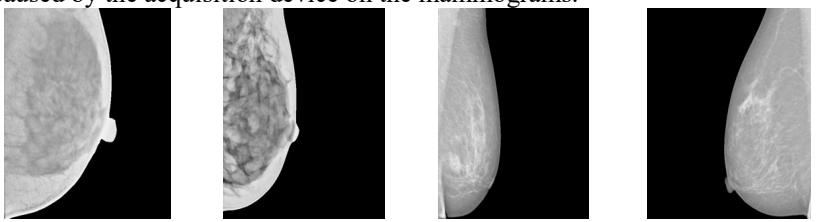

(a) CC- Right (b) CC- Left (c) MLO- Right (d) MLO- Left

Figure 3.10 Result of performing gamma correction

UTV image histogram equalization

After gamma correction, the CLAHE contrast equalization algorithm is used to achieve optimal image contrast. CLAHE is an improved variant of the AHE (Adaptive Histogram Equalization) algorithm [138] . CLAHE is commonly used in medical imaging to improve the quality of complex structures [139] .

The result of this step is shown in **Error! Reference source not found.**3.11 . The difference can be clearly seen when comparing the image before and after brightness adjustment.

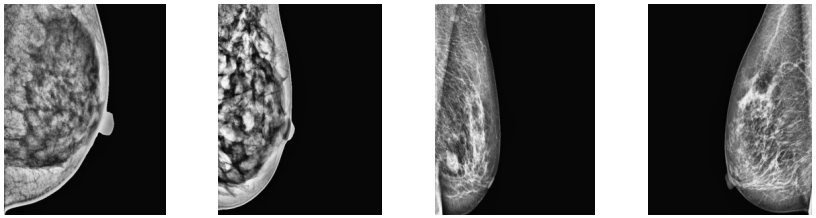

(a) Right CC (a) Left CC (a) Right MLO (a) Left MLO

Figure 3.11 Chart balancing using CLAHE

CHAPTER 4 IMAGE FEATURE EXTRACTION AND ROI PROCESSING FOR BREAST CANCER CLASSIFICATION

4.1 UTV IMAGE SEGMENTATION TO EXTRACT ROI REGIONS

In the UTV image classification system, all images need to be processed to extract the largest ROI, focusing on the lesion area to increase accuracy and reduce computation time. Otsu algorithm is used to segment the image, then only keep the largest ROI based on pixel density, remove the smaller ROIs. This ROI is multiplied with the original image to obtain the lesion area, then normalized and adjusted as illustrated in Figure 4.2.

Figure 41 Q process of extracting the largest ROI region

Figure 4.3 shows the result of extracting the largest ROI region, in which unwanted components and image background have been removed.

Benign tumors

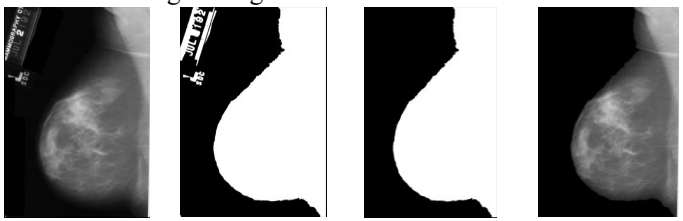

(a1) (a2) (a3) (a4)

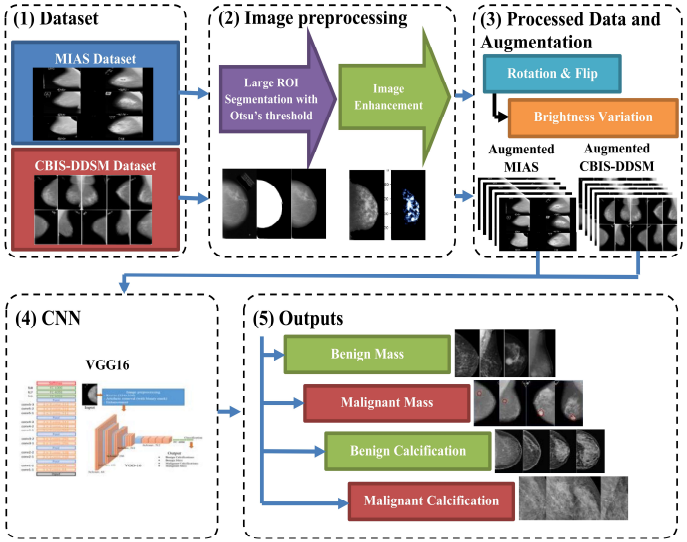

Figure 5. 1Classification block diagram and workflow: (1) two DL sets with four sets of breast lesion images; (2) Segmented images to find the largest ROI and enhanced; (3) Enhanced images from the largest ROI images; (4) and (5) VGG16 with four outputs for breast lesion classification.

This section evaluates the accuracy of VGG16 on three input image sets: without Otsu segmentation, with only Otsu segmentation, and the largest ROI from Otsu segmentation. The mammogram data are obtained from CBIS-DDSM and MIAS, where CBIS-DDSM (an enhanced version of DDSM) consists of 1,644 images of four types of breast lesions. All images are normalized to 224×224 pixels in size and RGB color code.

Classification results of lesion types using MIAS image set

On the CBIS-DDSM DL set, the model achieved an average accuracy of 95.23%, highest with MM (95.71%) and BM (95.58%). On the MIAS DL set, the average accuracy was 91.78%, outstanding in BM (93.16%) and BC (92.21%). The deviation mainly occurred between BM and MM, but the rate was low (<5%). This result confirmed the effectiveness and potential of the model.

Meanwhile, the CROI image set achieves an incremental accuracy of about 92.6% F1 score. This means that the Effi-cientNet-B7 model is very suitable for the CROI image dataset.

Table 4. 3. Comparison of classification accuracy between colored images and grayscale images

Photo type	Training accuracy (%)	Test accuracy (%)	F1 score (%)
Grayscale image	87.6	84.3	84.2
Coloring pictures	94.2	92.6	92.6

CHAPTER 5 UTV IMAGE CLASSIFICATION USING DEEP LEARNING NETWORKS AND REMOTE UTV DIAGNOSTIC SUPPORT SYSTEM USING DEEP LEARNING NETWORKS

5.1 CLASSIFICATION PROBLEM OF LESIONS BASED ON MIAS BREAST X-RAY IMAGE SET

Data were obtained from CBIS-DDSM and MIAS, then enhanced by rotation, flipping and brightness change with four lesion types (benign tumor, malignant tumor, benign calcification, malignant calcification). The images were processed by Otsu segmentation to select the largest ROI and fed into the VGG16 network, refined the last two layers and added the output layer. The classification performance was evaluated by confusion matrix [142].

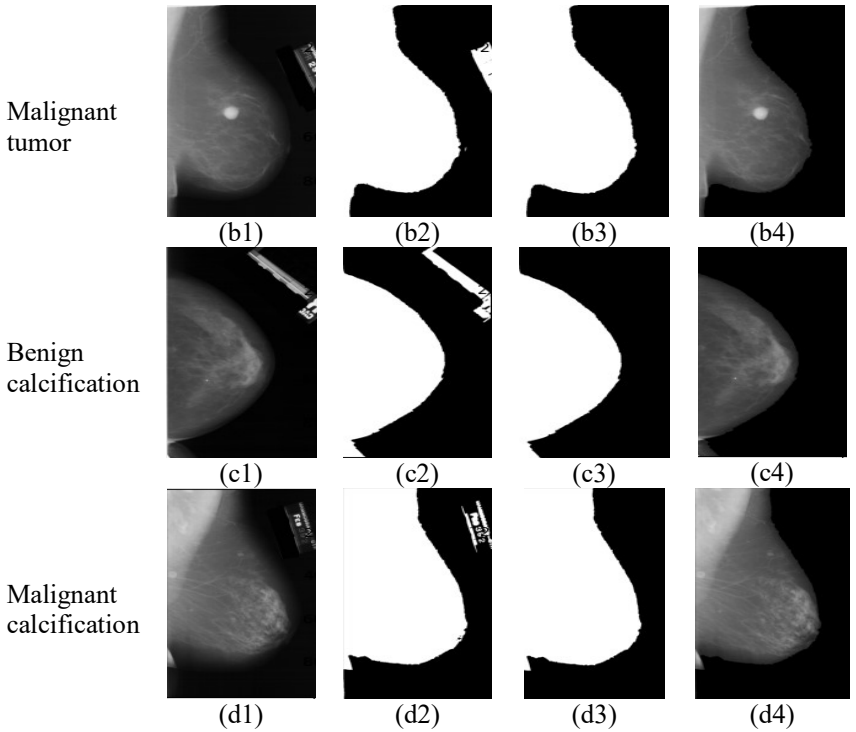

Figure 4.2 Description of ROI extraction based on largest contour and removal of unwanted components: (a1-a4) Original image of four breast lesions; (b1-b4) Segmented image using Otsu thresholding method (c1-c4) Binary image with largest ROI with removed unwanted components; (d1-d4) Original image with largest ROI without unwanted components

4.2 COLORING THE ROI AREA

UTV images are single-channel grayscale images, while EfficientNet is trained on three-channel color images. To take advantage of the model, the study developed a method of coloring ROI (CROI), highlighting tumors or calcifications. The algorithm consists of two steps: Identifying abnormal gray areas and Comparing the difference with the background using grayscale index and morphological transformations (TopHat, BlackHat). The result is converted into colored ICROI, which helps to increase the classification efficiency. Figure 4.5 illustrates 5 UTV images with different BIRADS levels, in which BIRADS 4 and 5 clearly show colored areas, highlighting signs of high-risk lesions.

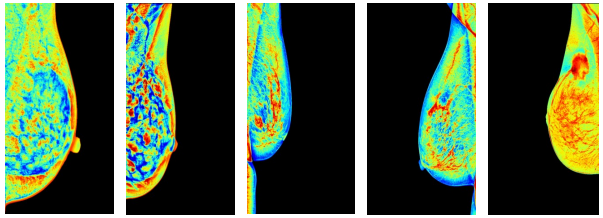

(a) (b) (c) (d) (e)

Figure 45. ROI colorization results for 5 images with BIRADS levels: (a) BIRADS 1; (b) BIRADS 2; (c) BIRADS 3; (d) BIRADS 4; (e) BIRADS 3image SEQ Hình * ARABIC \s 1

Figures 4.6 and 4.7 show that in cancer cases, the pixels corresponding to the grayscale range from about 50 to 130 in the histogram change abruptly from low to high, while in normal cases, the pixels in the same grayscale range increase slowly. Therefore, it is basically possible to judge the difference between the two types of breast images. However, the contrast values and the corresponding pixel counts provide more information for the assessment of breast disease status.

Table 4. 1. Feature extraction of cancer and normal cases

Case	*Cancer*		*Normal*	
	Contrast	***Number of pixels***	***Contrast***	***Number of pixels***
1	0.1927	558	0.0758	319
2	0.1478	417	0.0711	331
3	0.1582	484	0.0702	207
4	0.1419	402	0.0269	343
5	0.1501	601	0.0458	391
6	0.0817	513	0.0181	212
7	0.2799	527	0.0584	388
8	0.2483	560	0.0855	326.
9	0.1185	442	0.0746	98
10	0.1455	420	0.0295	77

Table 4.1 shows the contrast values corresponding to the average number of pixels of cancer images and normal images in the grayscale range from 0.2 to 0.3 on the histogram. Obviously, the contrast values in normal images range from 0.0181 to 0.0855, while in cancer images they range from 0.0817 to 0.2799. In addition, the number of pixels corresponding to the image contrast of 10 images for each type is also different. Specifically, the number of pixels in cancer images ranges from 402 to 601, while in normal images it ranges from 77 to 391.

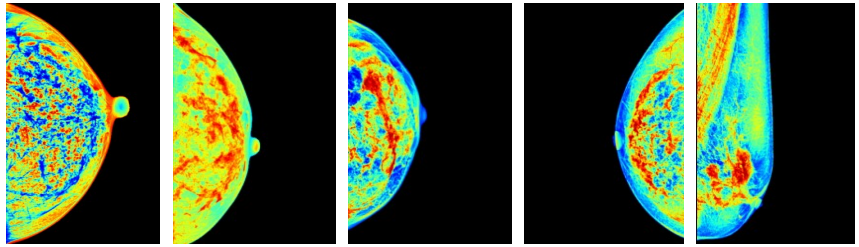

(a) (b) (c) (d) (e)

Figure 4. 10. Illustration of four different lesion types of images with CROI: (a) Not detected; (b) Tumor; (c) Calcification; (d) Tumor & Calcification.

Figure 4.15 shows that CROI highlights lesions with color (red for tumors, blue and red for calcifications), which clearly distinguishes them from non-lesion images. When comparing the confusion matrices (Figures 4.16 and 4.17), the EfficientNet-B7 model achieves higher accuracy with colored ROI images (92.6%) than with gray ROIs (84.3%), demonstrating the effectiveness of the coloring method.

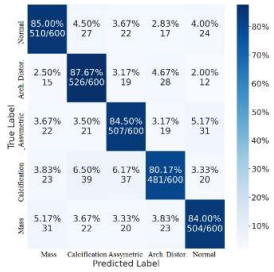

Figure 4.11 Confusion matrix for evaluating classification performance for grayscale image sets

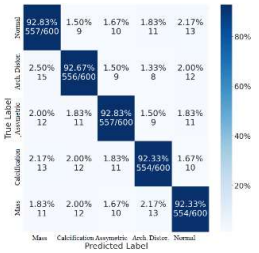

Figure 4. Confusion Matrix results for 12classification performance for colored image sets

In Table 4.3, the simulation results show that the proposed image preprocessing methods significantly increase the overall accuracy of classifying breast lesion image sets. Specifically, the GROI image set produces a higher accuracy of 82.3% compared to the original image set which only achieved 74.3%.

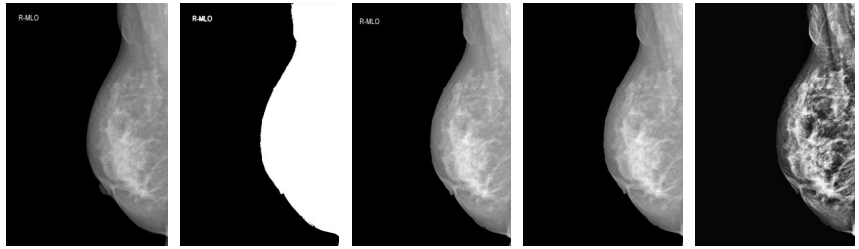

(a) (b) (c) (d) (e)

Figure 4. 8. Illustration of image processing: (a) Original image; (b) Image after applying mask with optimal threshold; (c) Segmented image; (d) Image after morphological operations and cleaning; (e) Image with GROI after post-processing.

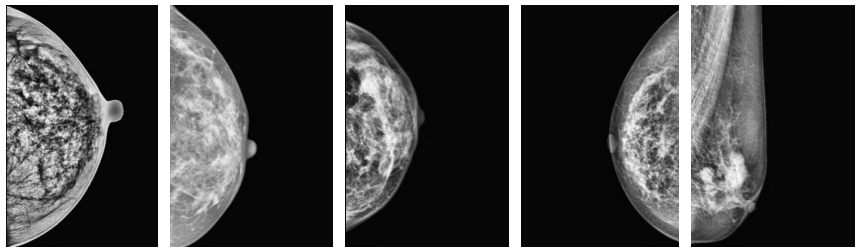

(a) (b) (c) (d) (e)

Figure 4. 9. Illustration of five image types with GROI and black background: (a) normal; (b) focal asymmetry; (c) structural deformation; (d) calcification; (e) tumor.

After generating the GROI images, these images were converted into CROI images using a coloring algorithm. Figure 4.15 illustrates the results of five types of color images with different types of lesions. It can be seen that the colored regions on the CROI are clearly different from the normal tissue regions. This means that the coloring in the CROI has highlighted some areas with a high risk of UTV. Therefore, these CROI images can provide high classification accuracy when used with the EfficientNet-B7 model.

UTV image classification based on GLCM features and SVM model

The image data exploited in this study are obtained from the Mini-DDSM dataset. [144] . The mammograms used are in 16-bit grayscale format, including 9,684 images of 3 types: benign, cancer and normal. This study uses a part of the Mini-DDSM dataset for processing, feature extraction and classification of breast cancer.

Table 4. Representation of training 2images

Data set	Cancer	Normal
Train	100	100
Test	50	50

UTV images were analyzed for feature extraction using GLCM and this enabled detection of potential breast cancer. best for SVM classification.

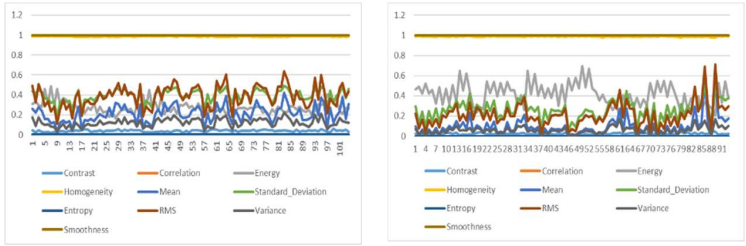

(a) (b)

Figure 4.4 Statistical features of breast images using GLCM: (a) Features of normal images; (b) Features of cancer images

In the testing step after SVM classification for the tested data, the calculation to find out the accuracy and sensitivity of the system is done by applying the confusion matrix as shown in figure 4.10.

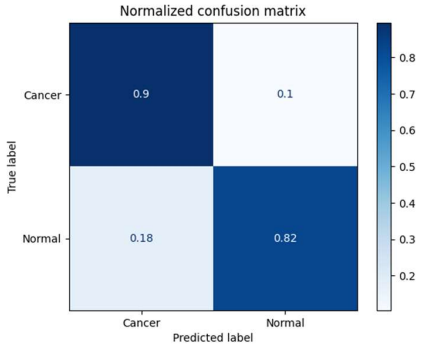

Figure 4.5 Confusion Matrix

With the cancer image dataset of 50 images, 45 images were classified correctly with 90% accuracy. In addition, with 50 normal images, the system classified 41 images correctly, accounting for 82%. Thus, the average accuracy for both types was 86%. These results demonstrate the significance of the features found in classifying UTV images [145] .

UTV image classification based on ROI region

The UTV image set is divided into five types of lesions: mass, calcification, architectural distortion, asymmetry, and normal. To classify these image sets using the EfficientNet-B7 model, the input data will be processed in two steps: extracting GROIs in the image sets; converting CROIs to CROIs as illustrated in Figure 4.11 [143] . In addition, the data sets will be balanced by increasing the number of images, while randomly reducing the sets with too large sizes.

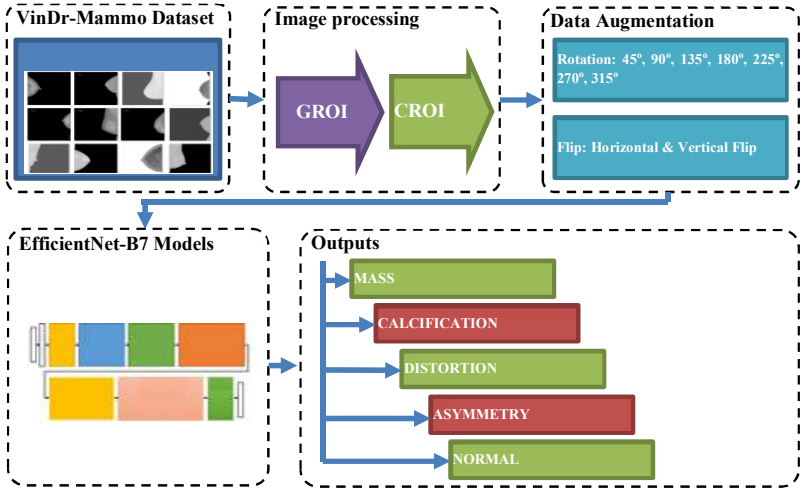

Figure 4. Overall flowchart of 6ROI-based UTV image classification method

In this study, the VinDr-Mammo dataset [135] is used. This dataset consists of 5,000 mammograms, corresponding to 20,000 images, each of which generates 4 breast images: right Cranial-Caudal (CC), left CC, right Mediolateral-Oblique (MLO), and left MLO, as illustrated in Figure 4.12.

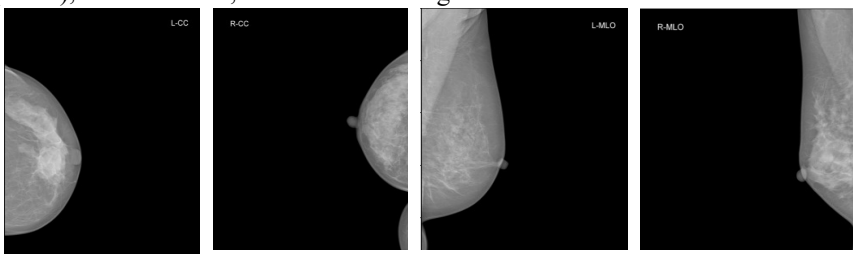

(a) **(b)** **(c)** **(d)**

Figure 4. 7. Set of 4 sample mammograms for one scan in the VinDr-Mammo dataset: (a) Left CC; (b) Right CC; (c) Left MLO; (d) Right MLO.